Chemical Engineering Science 193 (2019) 325–335

Contents lists available at ScienceDirect

Chemical Engineering Science

journal homepage: www.elsevier.com/locate/ces

Numerical simulation of dynamic behavior of compound droplets on solid surface in shear flow by front-tracing method

Xinglong Shang, Zhengyuan Luo, Bofeng Bai *

State Key Laboratory of Multiphase Flow in Power Engineering, Xi'an Jiaotong University, Xi'an 710049, China

HIGHLIGHTS

- A model was developed for compound droplet involving moving contact line problem.
- We observed several interesting events of droplet sliding, detachment and pinch-off.
- Capillary numbers of inner and outer droplet significantly affect droplet dynamics.
- Effects of surface tension and inner droplet radius on droplet were studied.

ARTICLE INFO

Article history:
Received 16 May 2018
Received in revised form 8 September 2018
Accepted 15 September 2018
Available online 17 September 2018

Keywords:
Compound droplets
Dynamic behavior
Moving contact line
Detachment and pinch-off
Multiphase flow
Front-tracking method

ABSTRACT

The dynamic behavior of compound droplets on the wall of a rectangle channel by the action of an imposed shear flow is simulated using our developed three-dimensional front-tracking method combined with generalized Navier boundary condition. The validity of the present method was confirmed by comparing results of the compound droplet spreading under gravity force with analytical solutions. To determine the physical condition required for detaching/pinching-off the compound droplet, we have performed a large number of simulations with varying capillary numbers of two interfaces and obtained a phase diagram of compound droplets on solid surface in shear flow. The deformation and motion of the compound droplet including its contact line motion are investigated. It is found that the behavior of the compound droplet is controlled by two dimensionless parameters, the capillary numbers of the outer interface and the inner interface. Moreover, we also analyze the deformation and migration of the inner droplet and discuss its effect on the compound droplet. The simulation demonstrate that the lateral migration of the small inner droplet could accelerates the pinch-off process and the large inner droplet could promote the detachment for a moderate capillary number of the outer interface.

1. Introduction

Compound droplets are the most common types with wide-ranging applications in targeted drug delivery (Engel et al., 1968; Langer, 1998), cosmetic (Vasudevan and Naser, 2002), microfluidics (Shintaku et al., 2007; Utada et al., 2005) and modeling of biological cells (Hochmuth et al., 1993). The compound droplets suspend in a continuous phase has been observed in the phase separation (Smith et al., 2000) as well as the displacing process during enhance oil recovery (EOR) (Chen et al., 2011). Because of a small droplet encapsulated by another immiscible fluid or thin membrane, the compound droplet can exhibit various behaviors when it under an external flow field confined in a channel (Bazhlekov et al., 1995; Smith et al., 2004; Stone and Leal, 1990). The study of its deformation and motion is fundamental to understanding the manipulation mechanism of compound droplets appeared in a variety of industrial processes.

The dynamics of free compound droplets in an external flow have been widely studied. Most work dealt with the hydrodynamics of compound droplet in confined channel and focus on the achievement of critical boundary between typically behaviors including swing, tumbling and tank-treading. The influences of inertia (Bazhlekov et al., 1995), viscoelasticity (Luo et al., 2015), initial shape (Luo and Bai, 2016; Palaniappan and Daripa, 2000) and interfacial properties (Hua et al., 2014) have been reported in the previous literatures. Besides, the breakup of compound droplets is of considerable interest in many applications. A series of breakup scenarios for free compound droplets with uniform surface tension have been presented (Smith et al., 2004; Stone and Leal, 1990). However, less work has been done on the hydrodynamics if compound droplets attached directly to a rigid wall.

* Corresponding author. Tel.: +086 029-82665316.
E-mail address: bfbai@mail.xjtu.edu.cn (B. Bai).

https://doi.org/10.1016/j.ces.2018.09.021
0009-2509/

Motivated by the mentioned above, a further investigation for what behavior of the compound droplet, for instance, oil-water double emulsion adhering to the reservoir rock in EOR (Dimitrakopoulos and Higdon, 1998), is greatly important in a variety of applications. The wall not only acts as a boundary to confine the flow but its wettability should also be considered as an additional effect in the dynamics of the droplet. In this case, the moving contact line is a crucial factor to affect the performance of those applications mentioned above. The typically scenarios of morphology, including droplet sliding, detachment and pinch-off have been found for a homogenous droplet under an external flow (Ding et al., 2010; Spelt, 2006; Sugiyama and Sbragaglia, 2007). Besides, several numerical methods have been developed to model the hydrodynamics of homogeneous droplet involving the moving contact line problems, in which the effects of wettability including the contact angle hysteresis (Park and Kang, 2012; Spelt, 2005; Wang et al., 2013) caused by the chemical or physical heterogeneity have also been considered. The effect of fluid inertia, interfacial tension and wettability on the critical transition condition between different behaviors for a homogeneous have been investigated (Dupont and Legendre, 2010; Fang et al., 2008).

Compared with a homogenous droplet, the interaction between the two interfaces leads the compound droplet to exhibit various morphologies. We have found the deformation of the overall compound droplet is smaller than that of the homogeneous one and revealed the underlying mechanism (Luo et al., 2015). Very little is known about the influence of moving contact line on the compound droplet. There were only a few studies of compound droplet involving the moving contact line problem, for instance compound droplet spreading or impacting on a wetting substrate. Gao and Feng (2011) considered the spreading and breakup of a compound droplet on a partially wetting substrate and observed various scenarios of morphological change. The impacting of a two-dimensional compound droplet has been performed using a front-tracking/finite-difference method by Tasoglu et al. (2010). Very limited effort has been contributed to the study of compound droplets sliding, detachment and pinch-off, especially when it is displaced by another fluid.

In the present paper, we perform a numerical simulation to investigate the deformation and motion of a compound droplet on a wall with considering contact angle hysteresis. The main purpose is to explore various scenarios of morphological transition of compound droplets. After validating the computational model against the theoretic solution of droplet spreading. Further simulations are performed to study effects of governing non-dimensional numbers, i.e., capillary numbers of the inner and outer interface and radius ratio of inner droplet to outer droplet, on the behavior of compound droplets on solid surface in shear flow. A phase diagram showing the clearly transition between the sliding, detachment and pinch-off regimes is obtained. Then we analyze the deformation and motion of the compound droplet including the contact line motion. It is found that the inner droplet effect can be ignored with a small capillary number of the outer interface, even for the large inner droplet. We demonstrate that the compound droplet pinch-off is more likely to be observed at relative large capillary number of the outer droplet and small capillary number of the inner droplet.

2. Problem specification and formulation

We consider a compound droplet consist of an outer interface with an equivalent radius R_2 based on its volume, which enclosing a free droplet of radius φR_2 under a simple shear flow. Initially, the inner droplet locates at the central of the internal region inside the outer droplet, i.e., $x = 0.4L_x$, as shown in Fig. 1. The outer interface inserts into the wall (whose static contact angle is θ_e) with a

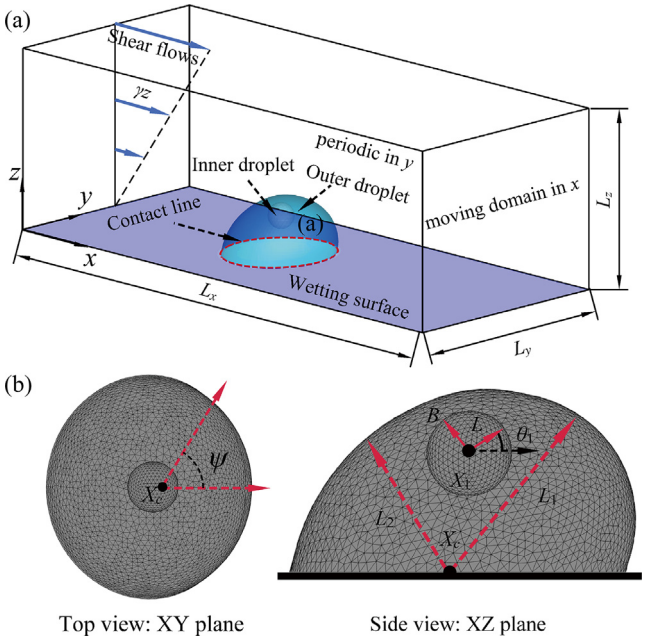

Fig. 1. (a) Schematics of a compound droplet adhering to a wall of the confined channel under a shear flow. The computational domain size $L_x \times L_y \times L_z$ is $14R_2 \times 5R_2 \times 4R_2$, where R_2 is the equivalent radius of outer droplet, inside which a free droplet with radius φR_2 is suspended. (b) Geometric parameters to characterize the deformation and motion of the compound droplet, where L_1 and L_2 are the maximum and minimum distances from the centroid X_c of the wetting area to the outer interface, respectively, X_1 is the centroid of the inner droplet.

uniform initial contact angle θ_0. Unless stated otherwise, the fluids inside and outside the compound droplet are taken as incompressible, mutually immiscible and Newtonian fluids with the constant density ρ_0 and viscosity μ_0. Because of the droplet size we focus on is micrometer, the gravity can be safely neglected. The geometric parameters L_1 and L_2 are used to characterize the deformation of compound droplet, where L_1 and L_2 are the maximum and minimum distances between the central of wetting area to the outer interface, respectively, as seen in Fig. 1. The status of the inner droplet is characterized by the deformation index D_1 (= $(L - B)/(L + B)$) and the orientation angle θ_1, where L and B are the major and minor axes in the shear plane of the ellipsoid with the same inertia tensor as that of the deformed droplet, respectively, and θ_1 is the angle between the major axis of the ellipsoid and the x-axis (i.e., the flow direction). Several impact parameters potentially influence the behaviors turning of compound droplets, e.g., surface tension, radius of the inner droplet, slip parameter and viscosity, etc. In this work, we focus on the effects of capillary number of the outer interface and the radius ratio of the inner droplet to outer droplet on the deformation and motion of the compound droplet.

The two-phase flow over the entire computational domain is governed by a single set of continuity and Navier–Stokes equations as follow:

$$\nabla \cdot \mathbf{u} = 0, \tag{1}$$

$$\frac{\partial(\rho\mathbf{u})}{\partial t} + \nabla\cdot(\rho\mathbf{u}\mathbf{u}) = -\nabla p + \nabla\cdot\mu\left(\nabla\mathbf{u} + \nabla\mathbf{u}^T\right) + \int_{A_1}\sigma_1\kappa\mathbf{n}_f\delta(\mathbf{x}-\mathbf{x}_f)dA_1 + \int_{A_2}\sigma_2\kappa\mathbf{n}_f\delta(\mathbf{x}-\mathbf{x}_f)dA_2 \tag{2}$$

where $\mathbf{u} = (u, v, w)^T$ is the velocity vector, t is the time, p is the pressure, and μ and ρ are the discontinuous viscosity and density field of the two-phase fluids, respectively. κ is the curvature, $\mathbf{n}_f$ is the outer unit vector normal to the interface, σ_1 and σ_2 are the surface

tension coefficients of the inner interface A_1 and the outer interface A_2. The last two surface tension terms in Eq. (2) are obtained from the Lagrangian grid points and are distributed to the surrounding Eulerian grid points using a smoothed approximation of the Dirac Delta function δ, in which $\mathbf{x}_f$ and $\mathbf{x}$ are points at the interface and in the surrounding fluid, respectively. The interface merging or breakup is not considered in the present study, thus the density ρ and viscosity μ vary discontinuously across the interfaces and can be determined by the indicator function I

$$\mu = \begin{cases} \mu_0 + \mu_0(k_{\mu 2} - 1)I, & \text{if } I \leqslant\leqslant 1, \\ \mu_0 k_{\mu 2} + k_{\mu 2}\mu_0(k_{\mu 1} - 1)(I-1), & \text{if } 1 < I \leqslant\leqslant 2, \end{cases}$$
$$\rho = \begin{cases} \rho_0 + \rho_0(k_{\rho 2} - 1)I, & \text{if } I \leqslant\leqslant 1, \\ \rho_0 k_{\rho 2} + k_{\rho 2}\rho_0(k_{\rho 1} - 1)(I-1), & \text{if } 1 < I \leqslant\leqslant 2, \end{cases} \tag{3}$$

where $k_{\mu 1}$ and $k_{\rho 1}$ are the viscosity and density ratios of fluid between the inner droplet (i.e., $I = 2$) and encapsulating droplet (i.e., $I = 1$), $k_{\mu 2}$ and $k_{\rho 2}$ are the viscosity and density ratios of fluid between the encapsulating droplet (i.e., $I = 1$) and the surrounding fluid (i.e., $I = 0$), as seen in Fig. 1. The indicator function is computed following the procedure described by Tryggvason et al. (2001). For the outer interface, the discontinuity of outer unit vector normal to the interface is distributed onto the Eulerian grid points near the interface resulting in the gradient field

$$\mathbf{G} = \nabla I_2 = \int_A \mathbf{n}_f \delta(\mathbf{x} - \mathbf{x}_f) dA, \tag{4}$$

which is nonzero only in the vicinity of outer interface. Then the indicator function I_2 can be obtained by solving the separable Poisson equation

$$\nabla^2 I_2 = \nabla \cdot \mathbf{G}. \tag{5}$$

Eq. (5) only needs to be solved efficiently near the interface. Then the procedure described above in Eqs. (4) and (5) is repeated, and the indicator function I_1 can be obtained basing on the inner interface position. Finally, the indicator function $I = I_1 + I_2$ in Eq. (3) is used to update the material field.

The dynamics of the moving contact line is prescribed by imposing a slip boundary according the generalized Navier boundary condition (GNBC), (Qian et al., 2003a) in which the slip velocity $\mathbf{u}_{slip}$ on the solid surface is proportional to the viscous shear stress on the wall $\boldsymbol{\tau}^{vis}$ and the unbalanced Young's stress $\boldsymbol{\tau}^{Y}$:

$$\beta' \mathbf{u}_{slip} = \boldsymbol{\tau}^{vis} + \boldsymbol{\tau}^{Y}. \tag{6}$$

Here, β' is a coefficient with the form μ/λ (λ is the slip length defined as the as a vertical distance relative to the wall where the tangential velocity component vanishes). Note that the unbalanced Young's stress term is related to the surface tension of the interface in contact with the wall and dynamic contact angles, which is zero in the region far from the contact line.

3. Numerical method

3.1. Front-tracking method

A three-dimensional front-tracking/finite-difference method is developed to track the deformed fluid-fluid interface. Several general procedures for the front-tracking method to model the dynamics of homogeneous droplets with MCL has been previously described in Refs. (Huang et al., 2004; Muradoglu and Tasoglu, 2010; Yamamoto et al., 2013). In the present method, we introduce the GNBC to the front-tracking method and further improve its ability and stability in tracking the complicated two-dimensional contact line.

We follow the procedure proposed by Esmaeeli and Tryggvason (1998) to compute the surface tension in the Eq. (1). Generally, the surface tension is converted to a contour integral over the edges of a surface segment instead of the surface integral of the curvature based on Stokes' theorem. The surface tension on the interface is then interpolated onto the Eulerian grid by using the approximated delta function δ.

$$\int_{A_2} \sigma_2 \kappa \mathbf{n}_f \delta(\mathbf{x} - \mathbf{x}_f) dA_2 = -\sigma_2 \int_C \mathbf{t} \times \mathbf{n}_f \delta(\mathbf{x} - \mathbf{x}_f) dl, \tag{7}$$

where $\mathbf{t}$ and dl are the unit direction vector and length of the edge of triangular mesh. Note that surface tensions acting on the contact line is considered in the GNBC (Eq. (6)) as the boundary condition. Thus, surface tension term in the governing equation does not contain the force acting at the contact line. The new position of the interface can be updated by using its velocity $\mathbf{u}_f$ interpolated from the velocities of the adjacent stationary grid points.

$$\mathbf{u}_f(\mathbf{x}_f) = \sum \delta(\mathbf{x} - \mathbf{x}_f)\mathbf{u}(\mathbf{x}) h_x h_y h_z, \tag{8}$$

where h_x, h_y, h_z are the uniform intervals of Eulerian grid along x-, y- and z-aixs. In the present work, we use the following function to approximate the delta function:

$$\delta(\mathbf{x} - \mathbf{x}_f) = \delta(x - x_f)\delta(y - y_f)\delta(z - z_f). \tag{9}$$

Here, a cosine distribution function proposed by Peskin (2003) is chosen as the discretized form of function $\delta(r)$:

$$\delta(r) = \begin{cases} \frac{1}{4h}\left(1 + \cos\left(\frac{\pi r}{2h}\right)\right) & \text{if } |r| \leqslant 2h, \\ 0 \text{ if } |r| > 2h, \end{cases} \tag{10}$$

where h is the uniform interval of the Eulerian grid.

The interface is restructured at every time step in order to keep the Lagrangian grid point nearly uniform by deleting and splitting front elements that reach a prespecified limit in the same fashion as described by Tryggvason et al. (2001). Furthermore, a feature-preserving suboptimal Delaunay triangulation (S-ODT) is introduced to improve the quality of the Lagrangian grid, and the algorithm of local volume correction is implemented according to the work of Li et al. (2013).

The dimensionless governing equations are solved with characteristic quantities, i.e., length scale R_2, velocity scale γR_2, time scale γ^{-1}, where γ is the shear rate. In the present study, the diversity of viscosity and density throughout the two interfaces is not considered. The surface tension coefficient ratio of the inner interface to the outer interface is $\kappa = \sigma_1/\sigma_2$. The radius ratio of the inner droplet to the outer droplet is $\varphi = R_1/R_2$. The main non-dimensional numbers can be summarized as follow:

$$Re = \frac{\rho_0 \gamma R_2^2}{\mu_0},\ Ca_2 = \frac{\mu_0 \gamma R_2}{\sigma_2},\ We_2 = ReCa_2,\ Ca_1 = \frac{\varphi}{\kappa} Ca_2,$$
$$We_1 = ReCa_1. \tag{11}$$

The three-stage RKCN (Runge-Kutta/Crank-Nicholson) four-step projection method proposed by Ni et al. (2003) is employed to solve Eqs. (1) and (2) on a stationary collocated uniform Cartesian grid. The spatial derivatives are discretized using a second-order central difference scheme. To accelerate the convergence and to increase the time step size, the four-level multigrid technique and the alternating direction implicit scheme are used to solve the discretized pressure Poisson equation. In our method, the Crank–Nicolson semi-implicit technique is used for the diffusive term and the Runge–Kutta technique is employed for the convective and surface tension terms. The detailed numerical procedure can be found in the work of Luo et al. (2018).

3.2. Contact line dynamics

To solving the governing equation, in the present work, GNBC is applied on the grid of first layer near the wall. The general idea of GNBC is to calculate the slip velocity and use this velocity as the boundary condition. According to Eq. (6), the unbalanced Young's stress and viscous stress at the contact line must be computed. In front-tracking method, the interfacial force acting on the contact line (i.e., the non-zero net force of the surface tension at the three interfaces connected to the contact line) is computed and then converted to a stress distribution on the adjacent Eulerian grids of the solid surface. Thus, the boundary conditions for the velocity (i.e., slip velocity) on the solid surface can be written as:

$$\mathbf{u}_{\text{slip}} = \lambda \frac{\partial \mathbf{u}}{\partial z}\bigg|_{wall} + \frac{\lambda \tau^{Y}}{\mu} = \lambda \frac{\partial \mathbf{u}}{\partial z}\bigg|_{wall} + \frac{\lambda}{\mu}\sum_{k}\delta(x-x_k)\delta(y-y_k)\mathbf{f}_{\text{cl}}. \quad (12)$$

Here, $\mathbf{f}_{\text{cl}}$ is the wall tangent component of the interfacial force acting at the contact line marker point (x_{k}, y_{k}, 0), as seen in Fig. 2. Using Young's equation, $\mathbf{f}_{\text{cl}}$ can be expressed as:

$$\mathbf{f}_{\text{cl}} = \frac{1}{2}\sum_{\text{i}=1}^{2}(\mathbf{f}_{\text{wi}} + \mathbf{f}_{\text{i}}\cdot\mathbf{t}_{\text{wi}}) = \frac{1}{2}\sigma\sum_{\text{i}=1}^{2} l_{\text{i}}(\cos\theta_e - \cos\theta_{d,\,i})\mathbf{t}_{\text{wi}}, \quad (13)$$

where $\theta_{d,\,i}$ and l_i are the dynamic contact angle and length of the ith contact line element sharing the one contact line point, and $\mathbf{t}_{\text{wi}}$ is the unit normal of the contact line tangent to the wall. Because of the unbalanced Young's stress near the contact line is several orders of magnitude larger than the viscous stress due to the large slip velocity, the viscous stress term in Eq. (12) can be ignored in our present study (Qian et al., 2003b; Yamamoto et al., 2013). In the frame of front-tracking method, the calculation of Eq. (12) is dependent on the grid resolution. Therefore, the grid convergence of Eq. (12) has been validated, and the detailed result can be found in our previous work (Shang et al., 2018). Unless otherwise statement, λ is set to $0.01R$ to close to a practical value to fit the experimental data by Fermigier and Jenffer (1991). Note that the dynamic contact angle in the present study is obtained on the grid scale, which is different from the microscopic contact angle presented in the GNBC. To avoid the grid resolution dependency problems for moving contact line, a method applying Cox's relation (Cox, 1986) to match the two contact angles is proposed by Yamamoto et al. (2014). Under the present conditions, the capillary number $Ca_{\text{cl}} = \mu_0 u_{\text{cl}}/\sigma_2$ defined by the contact line velocity is in $O(10^{-2})$. The macroscopic and microscopic characteristic length scales are set to R and h_x, respectively. Then the term $Ca_{\text{cl}}\ln(R/h_x) = O(10^{-2})$ in Cox's relation can be safely ignored. Therefore, the grid-scale contact angle basing on Lagrangian grid can be directly used for the GNBC.

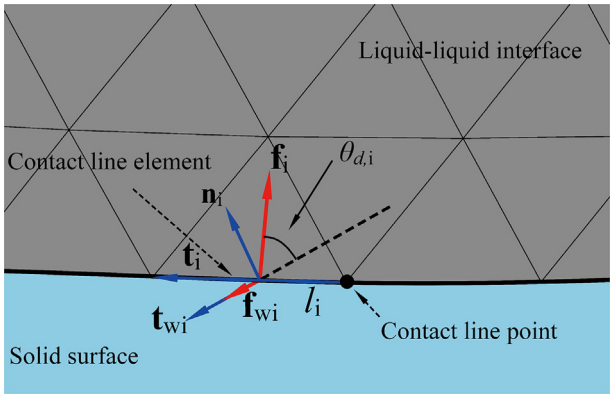

Fig. 2. Relation between contact angle and interfacial tension acting on the contact line element adjacent to the solid surface.

In the present study, contact angle hysteresis is considered for the solid surface, which is characterized by the advancing contact angle θ_A and the receding contact angle θ_R. When the dynamic contact angle θ_d exceeds the window of contact angle hysteresis, the unbalanced Young's stress tends to reshape the droplet interface to its equilibrium shape (i.e., θ_d trends to reach the equilibrium contact angle θ_A or θ_R), and the contact line moves, driving the droplet sliding on the solid surface. Thus, in the consideration of the hysteresis, the slip velocity on the solid surface can be determined based on the transformation of Eq. (12) by replacing the static contact angle to the corresponding θ_A or θ_R once the contact line moves. The modeling of contact angle hysteresis in the GNBC has been validation by simulating the deformation of droplet on a surface considering the hysteresis. Our results show that the contact line will move only if the dynamic contact angle is out of the window of hysteresis (Shang et al., 2018).

4. Results and discussion

4.1. Validation

In this section, the computation of surface tension and contact line model used in the present numerical method are first validated. The numerical performance of the three-dimensional front-tracking method for free compound capsules (an elastic capsule with a smaller capsule inside) in a simple shear flow has been validated (Luo and Bai, 2016; Luo et al., 2015). The GNBC is introduced into the four-step projection method after the intermediate velocity value is obtained at the second step. The validation of surface tension computation, i.e., the pressure jump and parasitic currents for a sessile droplet on solid surface has been conducted in the previous work. The results are accurate with a relative error of less than 1% and the maximum spurious velocity is in $O(10^{-3})$. Besides, the accuracy and convergence of the present numerical method for a homogeneous droplet spreading and sliding on the solid surface have been also recently demonstrated (Shang et al., 2018).

The evolution of the spreading radius R_s is obtained for different Eotvos number $Eo = \rho_L g R^2/\sigma$, which is based on equivalent radius R and the liquid density ρ_L and the surface tension σ. If the droplet changes towards a "pancake" shape driven by the gravity force, the driving force was balanced against dissipation at the contact line. In this case, as seen in Fig. 3(a), a scaling law with $R_s/R \sim t^{1/7}$ is in a good agreement with that of ours as reported by Ehrhard and Davis. (Ehrhard and Davis, 1991). For $Eo \leq 1$, the state-steady height of the droplet is controlled by the static contact angle. Then, the nondimensional h/R is calculated as follows:

$$\frac{h}{R} = \frac{R_0}{R}(1-\cos\theta_e)\sqrt{\frac{\pi}{2(\theta_e - \sin\theta_e\cos\theta_e)}}, \quad (14)$$

where R_0 and R are the initial and equivalent radii of the droplet, respectively. For $Eo \geq 1$, h/R is directly proportional to the capillary length:

$$\left(\frac{h}{R}\right)_{\infty} \approx \frac{2}{\sqrt{Eo}}\sin\left(\frac{\theta_e}{2}\right). \quad (15)$$

Then the spreading of a compound droplet over a dry, smooth and flat solid surface under gravity is considered in this section. The non-dimensional computational domain is $L_x \times L_y \times L_z = 8 \times 8 \times 5$. Unless otherwise statement, the governing equations are resolved by a uniform Cartesian grid with non-dimensional resolution of $h_x = h_y = h_z = 1/18$. The non-dimensional time step $d(\gamma t)$ is set to 2×10^{-4}. Fig. 3(b) shows the evolution of h/R_2 of the droplet versus the Eotvos number for a hydrophobic wall ($\theta_e = 3\pi/2$). The results are found to be in very good agreement with the two

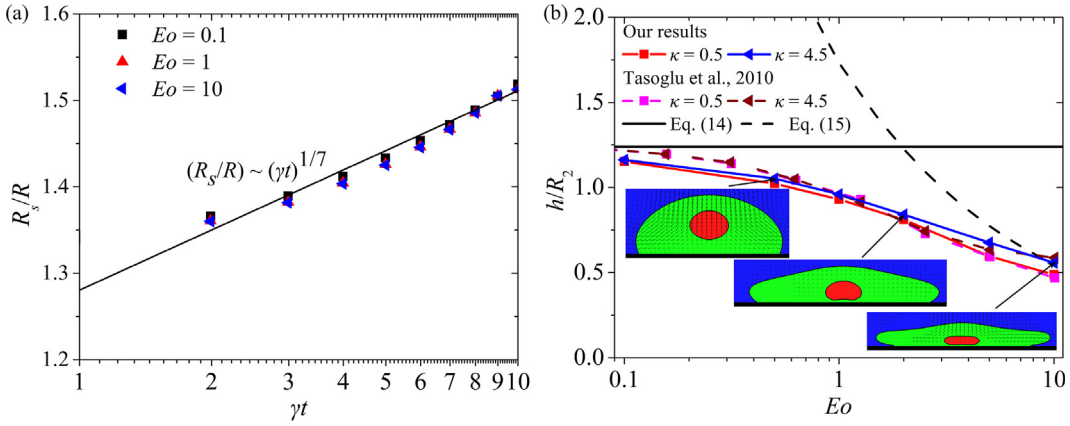

Fig. 3. (a) Spreading radius R_s/R of the homogeneous droplet without the inner droplet, and (b) the steady-state height h/R_2 of the compound droplet under gravity force.

solutions from Eqs. (14) and (15), respectively. For instance, when κ is 4.5, the difference between the analytical solution and our computational result is less than 7% for $Eo = 0.1$ and 2% for $Eo = 10$, respectively. The numerical solution deviates significantly from the analytical solution for a large Eotvos number as κ increases. This conclusion can also be found in the work of Tasoglu et al. (2010) Besides, the computed normalized droplet height also show a well agreement with the numerical results, (Tasoglu et al., 2010) especially for the intermediate values of the Eotvos number.

4.2. Sliding, pinch-off and detachment

In the GNBC-based front-tacking method to solve the moving contact line problem, the contact line speed is directly prescribed according to GNBC, in which the dynamic contact angle model is used. In the following test cases, the effect of contact angle hysteresis is considered, and the advancing contact angle is $\theta_A = 2\pi/3$ and the receding contact angle is $\theta_R = \pi/3$. Unless stated otherwise, the computational domain is $L_x \times L_y \times L_z = 16R \times 5R \times 5R$, and all the

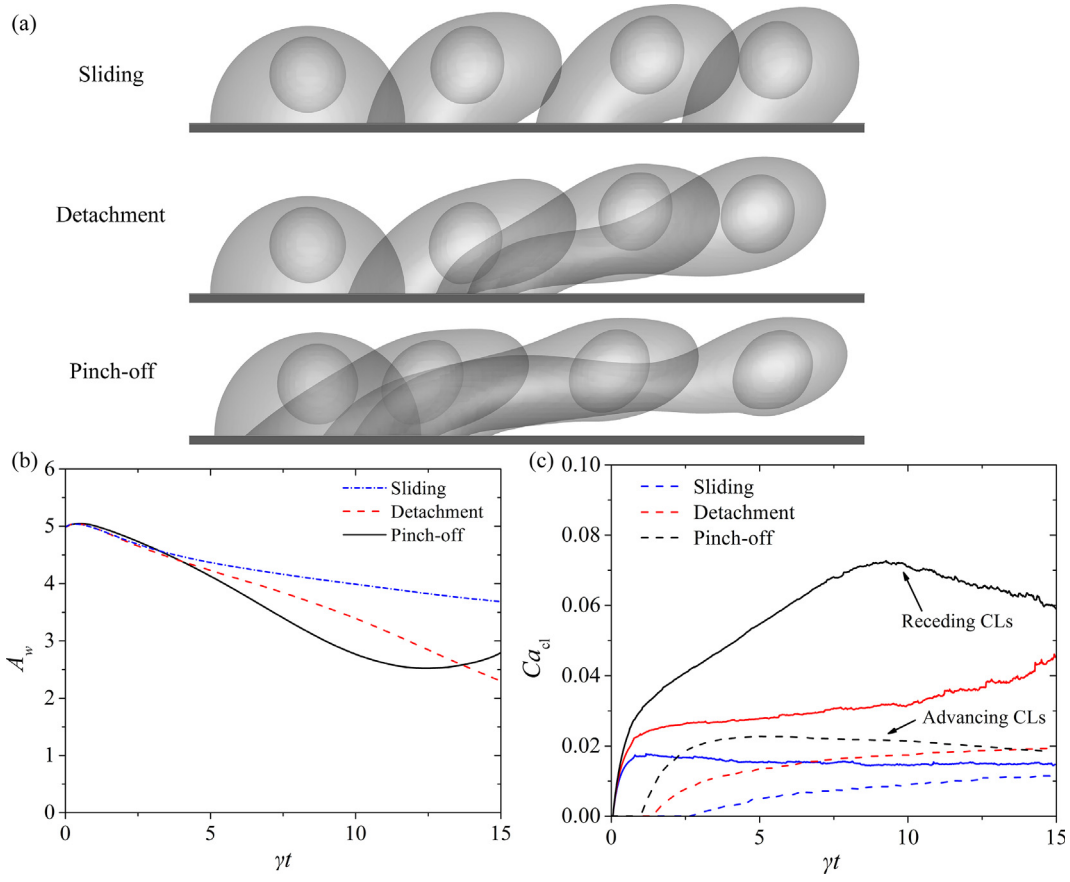

Fig. 4. (a) Successive snapshots, (b) the wetted area A_w and (c) the velocity u_{cl} of the contact line characterized by the capillary number $Ca_{cl} = \mu_0 u_{cl}/\sigma_2$ for the three scenarios of morphology of the compound droplet. Note that the results of droplet sliding, detachment and pinch-off are obtained at $(\varphi, Ca_2) = (0.5, 0.1)$, $(0.5, 0.15)$ and $(0.5, 0.3)$, where θ_0 and κ are setting to $\pi/2$ and 1, respectively.

results are obtained with $Re = 0.1$. Several factors may significantly affect the dynamics of the compound droplet, in the present study, we only consider the capillary number Ca_2 of the outer interface, the radius ratio φ of the inner droplet to the outer droplet and the surface tension coefficient ratio κ of the inner interface to the outer interface.

Because of the limitation of our method, the onset of pinch-off and detachment in our simulations cannot be captured, but obviously, it can be distinguished based on the information of deformation and motion of the contact line, as shown in Fig. 4(b) and (c). We classify the different morphologies by analysing the evolutions of wetted area A_w enclosed by the contact line and the capillary number Ca_{cl} defined by the velocity of contact line. Three morphologies of compound droplet including sliding, detachment and pinch-off are observed from our simulations as shown in Fig. 4(a). For the sliding droplet with a small Ca_2, the shape of compound droplet can reach a stable equilibrium. Accordingly, the small deformation of the outer interface lead to small difference in velocity between the two ends of contact line, i.e., the advancing and receding contact lines. This velocity difference along the contact line gives rise to a slight decrease of wetted area A_w as shown in Fig. 4(b). In contrast, detachment and pinch-off are preferred to occur with large velocity difference along the contact line, which results in significant decreasing of wetted area as the compound droplet sliding on the solid surface.

To further accurately distinguish the discrepancy in the three typical morphologies, Fig. 5 demonstrates the shape and motion of the compound droplet sliding on the solid surface versus time, i.e., L_1, L_2, and X_c (center of mass of the compound droplet). As the deformation is increased with increase of Ca_2, the outer droplet continues to elongate along the flow direction and the inner droplet gradually moves toward the downstream until the 'neck' of the slender ligament appears. Although our method cannot capture the onset of pinch-off, the result has shown that the resultant ligament is getting longer over time. A comparison of deformation for the three cases is shown in Fig. 5(a), L1 increases quickly and still has a tendency to increase. The pinch-off mechanism has been reported in other literatures for a homogeneous droplet (Ding et al., 2010). Fig. 5(c)–(e) show the streamlines at the location of the plane of shear, i.e., $y = 2.5$. Fig. 5(c) depicts the compound droplet sliding on the solid surface with a stable shape. In this case, a rotational flow is induced and the inner droplet moves in a rotational motion. In the case depicted in Fig. 5(d) and (e), the streamlines inside the compound droplet are inclined to the direction of flow. The inner droplet encounters an inclined shear flow and migrates away from the wall, in which case the elongation of the outer droplet is obviously shorter than the result of pinch-off case. Once A_w decreases to a magnitude that is equivalent to the size of 'neck', the compound droplet should be detached. Although the results discussed above are obtained for a wall with a relative large hysteresis, in addition to the detachment, various morphologies are also observed for the homogenous droplet on an ideal surface, even for the droplet with a pinned contact line. The dynamics of homogenous droplets in shear flow has also been investigated (Dimitrakopoulos, 2007; Ding et al., 2010; Ding and Spelt, 2007).

As discussed above, various behaviors of compound droplets are related to the relevant system parameters Ca_2, Ca_1. Firstly, we show a phase diagram that depicts the various regimes of compound droplets behavior in the (Ca_1, Ca_2) plane, which can be used to determine if a compound droplet remains stable, or undergoes detachment/pinch-off. Fig. 6 shows a phase diagram that depicts the various regimes of compound droplet behavior with initial contact angle $\theta_0 = \pi/2$ and $\kappa = 1$. The phase diagram indicates that the values of Ca_2 and Ca_1 required to achieve droplet detachment even

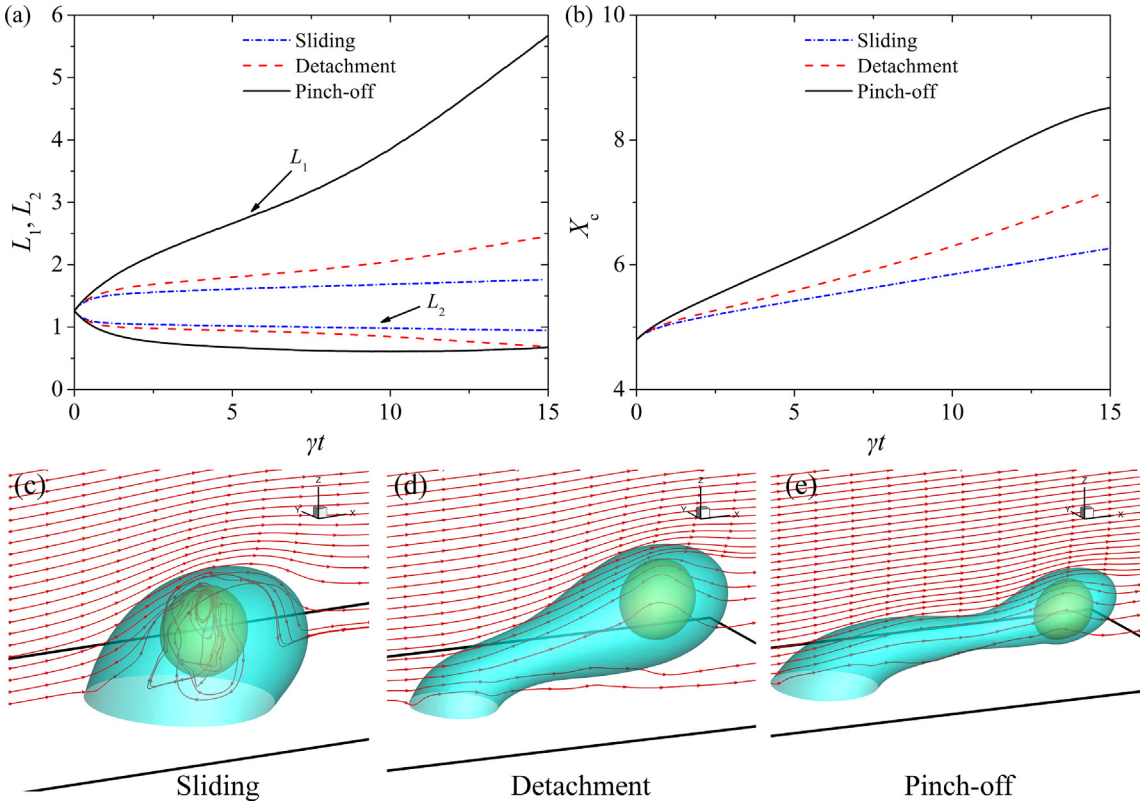

Fig. 5. Deformation and motion of compound droplets for three typical states including sliding, detachment and pinch-off, where L_1 and L_2 are the maximum and minimum distances from the outer interface to the centroid of the wetted region enclosed by the contact line, respectively, and X_c is the center of mass of the compound droplet. (c), (d) and (e) show the streamlines extracted from the inlet at the plane of $y = 2.5$.

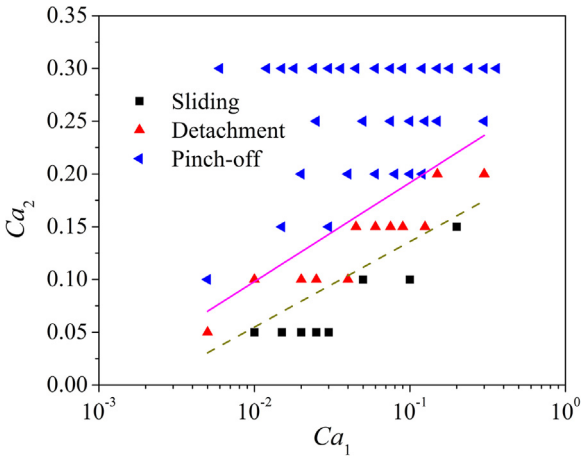

Fig. 6. Phase diagram representing the three typical regimes. The dashed line represents the boundary between the sliding and detachment and the solid line represents the boundary between pinch-off and detachment.

pinch-off. On the one hand, the compound droplet can be sliding on the solid surface with a relative small Ca_2 for a moderate Ca_1 (> 0.1). The deformation of the outer droplet is a prerequisite for the occurrence of pinch-off. For a given Ca_1, increasing Ca_2 would turn compound droplet from sliding into detachment even pinch-off. With increase of Ca_1, the effect of the inner droplet cannot be ignored. The presence of the inner droplet plays an important roles in the formation 'neck' of the slender ligament and the shrinking of wetted area, which are two key factors that determine whether the compound can be pinched-off or detached, respectively. It is found that pinching-off is preferred to occur with small Ca_1 and would turn into detachment with increase of Ca_1. For a moderate $Ca_2 > 0.25$, our result shows that the pinch-off will always occur and is independent of Ca_1.

4.3. Dynamics of contact line motion

In addition to the deformation, the dynamics of the contact line motion is also dominant for the compound droplet. Fig. 7 shows the evolutions of dynamic contact angle and velocity for the advancing (i.e., at the end of downstream) and the receding (i.e., at the end of upstream) contact lines at $\theta_0 = \theta_R = \pi/3$. Contact angle hysteresis effect causes the velocity of advancing contact line to show a zero value as seen in Fig. 7. The advancing contact line is pinned before the corresponding dynamic contact angle exceeds θ_R. For the sliding droplet, i.e., $Ca = 0.1$, in addition to the values of L_1 and L_2 as mentioned above, the contact line velocity can also reach a steady state, especially for the advancing contact line and the corresponding dynamic contact angle. The velocities of advancing and receding contact line increase because of the increased rate of change in dynamic contact angles with increase of Ca_2. Furthermore, the velocity difference between the advancing and receding contact line is also increased as Ca_2 increases, which is a key factor to determine the wetted area A_w. Besides, Fig. 7(b) and (c) demonstrate that the radius and surface tension of inner droplet seem to have no significant effects on the motion of the contact line. Thus, the contact line velocity is only independent of the capillary number Ca_2.

Fig. 8 shows the transient contact line profile and the corresponding dynamic contact angles distribution along the contact line. $\psi = 0$ is the position where the contact line advances, i.e., moves forward long the normal of the contact line tangent to the wall, and $\psi = \pi$ is the position where the contact line recedes. The value is in good agreement with that of the curve in Fig. 7, in which the dynamic contact angle at the receding contact line decreases with increasing Ca_2. However, the results for various values of φ and κ, as shown in Fig. 8(b) and (c), provide the evidence supporting the conclusion that the inner droplet has no significant effect on the motion of the contact line.

4.4. Deformation and motion of outer droplet

From the study of homogeneous droplets in the previous literatures, both contact-line movement and interfacial deformation are expected to play important roles. These two events may compete with each other, which are all affected by the surface tension, as seen in Eqs. (2) and (13).We fix the value of Ca_2 and decrease Ca_1 by setting various values of κ to study its effect on the deformation and motion of the compound droplet. Fig. 9 presents the result of the deformation and droplet motion as κ increases from 0.5 to 5 with $Ca_2 = 0.1$ and 0.3. For $Ca_2 = 0.1$ with $\varphi = 0.5$ as seen in Fig. 9 (a) and (c), L1 monotonically increases with decrease of Ca_1. Because of the existence of moving contact line, this tendency is completely different from the result of a free compound droplet suspended in a shear flow (Hua et al., 2014). Despite with a relative large inner droplet, the deformation of the compound droplet is still relative small. The rate of change with respect to time of X_c is approximately same with κ varying from 0.5 to 5. For a large value of $Ca_2 = 0.3$, the change of L_1 with increase of κ is different with the result at $Ca_2 = 0.1$. For a compound droplet with a large deformation of the outer interface, the surface tension of the inner

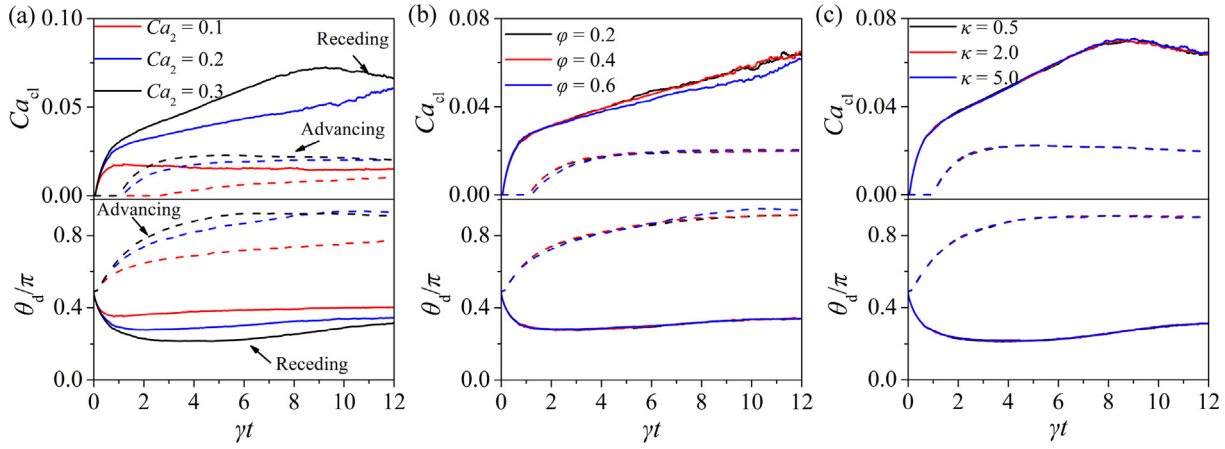

Fig. 7. Evolutions of contact line velocity and dynamic contact angle: (a) $\varphi = 0.5$ and $\kappa = 1$, (b) $Ca_2 = 0.2$ and $\kappa = 1$, and (c) $Ca_2 = 0.2$ and $\varphi = 0.5$.

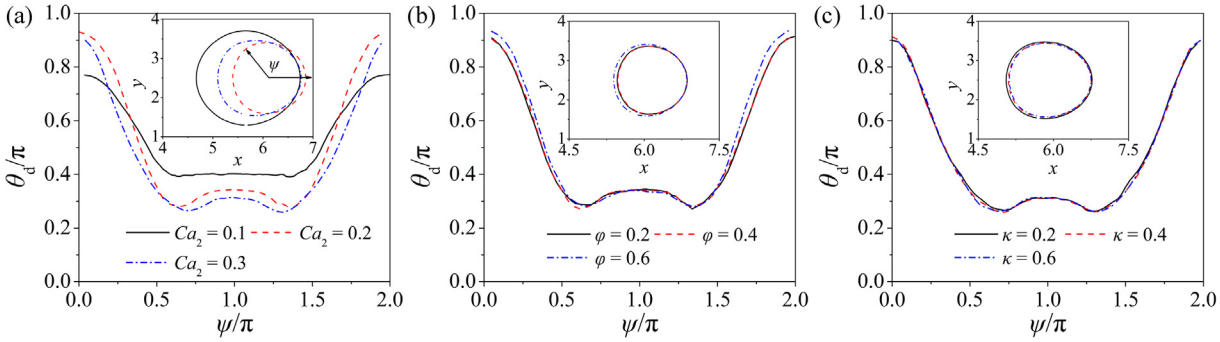

Fig. 8. Dynamics contact angle and contact line profile: (a) $\varphi = 0.5$ and $\kappa = 1$, (b) $Ca_2 = 0.2$ and $\kappa = 1$, and (c) $Ca_2 = 0.2$ and $\varphi = 0.5$.

droplet has complex effect on the evolution of L_1. As shown in Fig. 9 (b), the rate of change in L_1 is proportional to κ when its value is less than 2. However, this changing tendency is contrary as κ increases from 2 to 5. Furthermore, decreasing the surface tension of the inner droplet make it more inclined to the flow direction.

To investigate the effect of the outer interface with different deformability on the behavior of the compound droplet, we fix the surface tension of the inner interface and vary the Ca_2 by changing the values of κ. Fig. 10(a) and (b) show the time evolutions of L_1 and X_c for different values of Ca_2 with $\varphi = 0.1$ and 0.5, respectively. Similarly, the deformation of compound droplet increases as Ca_2 increases. With a small inner droplet, i.e., $\varphi = 0.1$, the value of L_1 from the compound droplet is approximately increased by three times as Ca_2 varies from 0.05 to 0.3 at $\gamma t = 12$. At the same time, Fig. 10(b) demonstrate that the velocity of compound droplet along the flow direction is decreased as φ increases to 0.5. However, the effect of φ on the deformation and motion of compound droplet can be ignored for $Ca_2 = 0.05$. In this case, a stable compound droplet can be observed to slide on the solid surface, even with a large inner droplet. Fig. 10(c) shows the snapshots of the compound droplet for different Ca_2 with various φ at the same time, i.e., $\gamma t = 12$. In general, the elongation of compound droplet along the flow direction decreases with increases of φ. Besides, the compound droplet is more likely to be detached/pinched-off with large φ and Ca_2, in which case the inner droplet undergo a strong inclined shear flow and the shape deviates from the sphere. For a moderate Ca_2, a large inner droplet can be able to decelerate the motion and deformation of the outer interface. After that, the deformed outer interface further affect the contact-line movement, then the contact line start to move (the dynamic

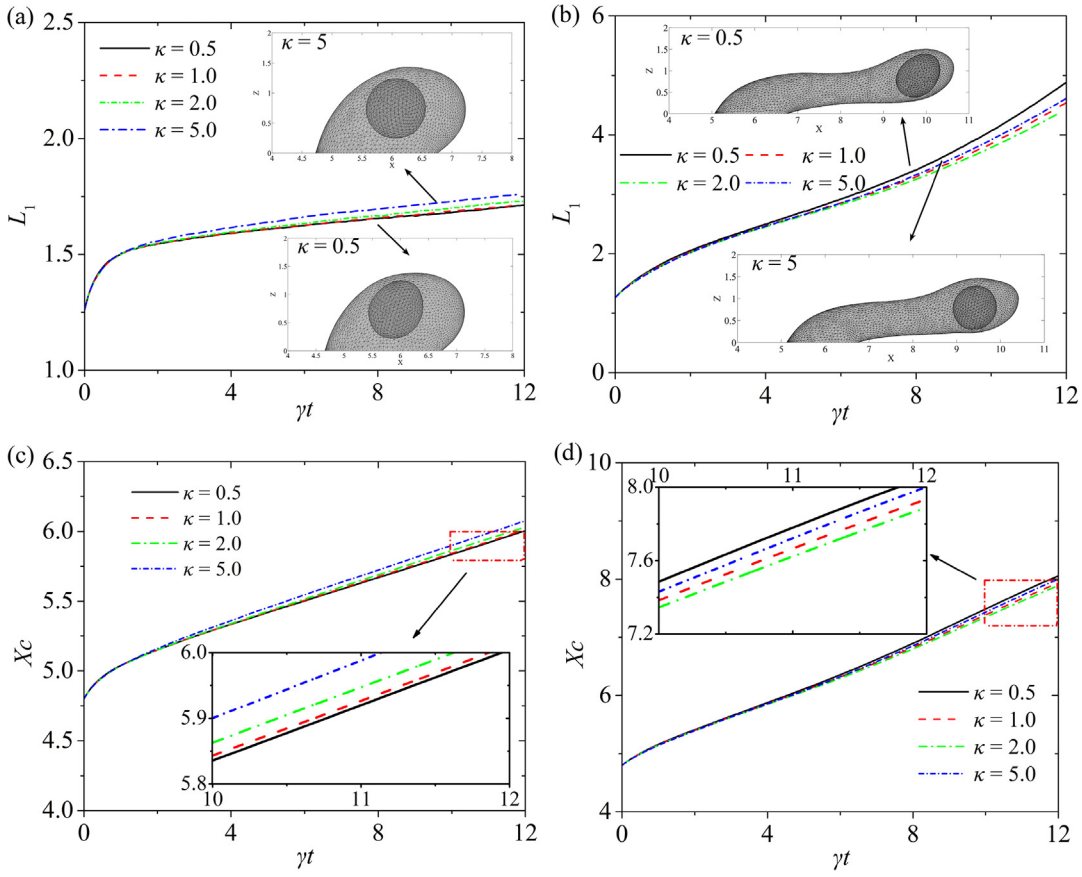

Fig. 9. Temporal evolutions of the deformation L_1 and the center X_c of mass of the compound droplet with $\kappa = 0.5$, 1, 2, and 5 for $Ca_2 = 0.1$ (i.e., (a) and (c)) and 0.3 (i.e., (b) and (d)), where the insert figures in (a) and (b) show the corresponding snapshots of the compound droplet representing by the Lagrangian grid at $\gamma t = 12$.

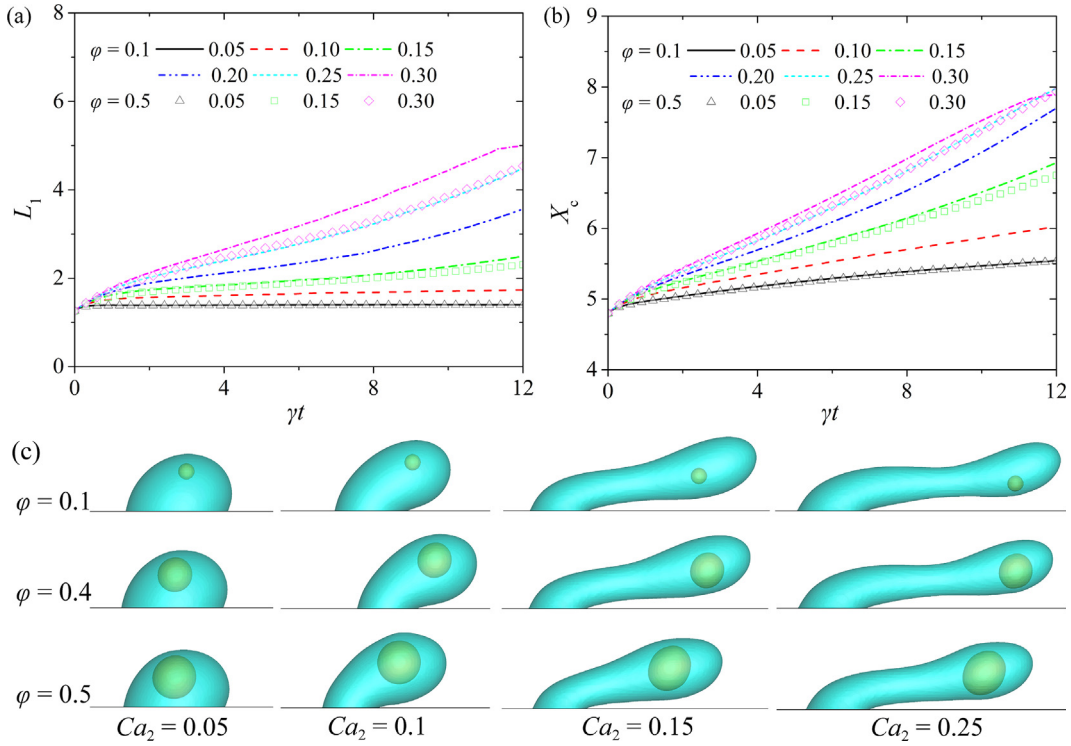

Fig. 10. Temporal evolutions of (a) the deformation L_1 and (b) the center X_c of mass of the compound droplet with varying Ca_2 = 0.05, 0.1, 0.15, 0.2, 0.25, and 0.3 with φ = 0.1, where the scatter plots represent the corresponding results at φ = 0.5. (c) Snapshots of the compound droplet at different Ca_2 with various values of φ at γt = 12.

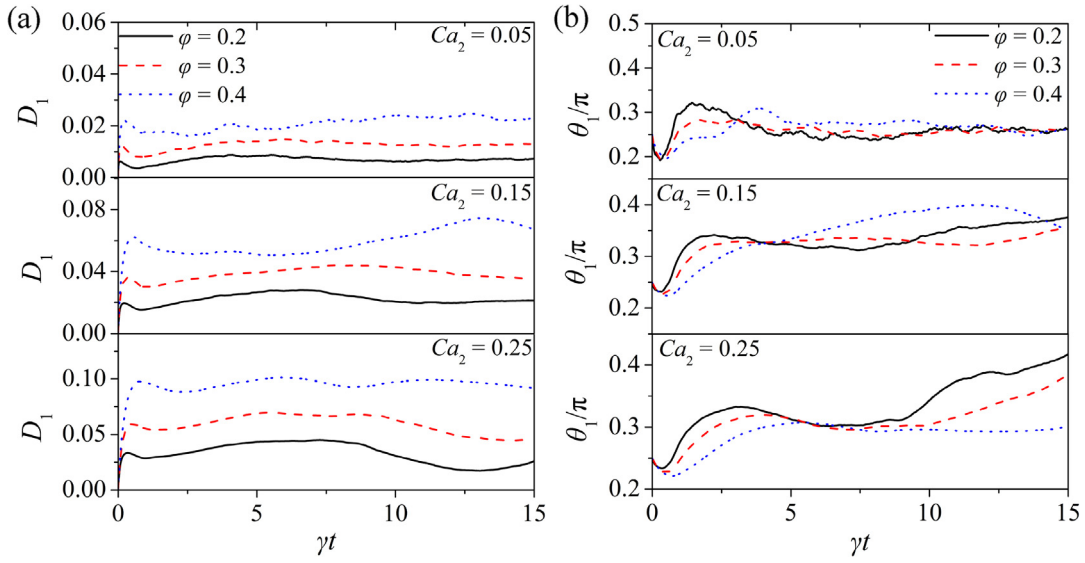

Fig. 11. Deformation (a) and orientation (b) of the inner droplet when Ca_2 = 0.05, 0.15 and 0.25 at different radius ratios with $\theta_0 = \pi/2$ and κ = 1.

contact angle exceeds the window of contact angle hysteresis) until all the dynamic contact angles reach their static values. The combined effects of the interface deformation and contact-line movement together govern the behaviors of the compound droplet.

4.5. Deformation and motion of inner droplet

As mentioned above, in addition to the deformation of the interfaces, the migration of the inner droplet also has a great effect on the behavior of the compound droplet. The induced shear flow in the region enclosed by the outer interface will accelerate the inner droplet moving away from the wall. Fig. 11 shows the evolution of deformation parameter D_1 and inclination angle θ_1 at different radii of the inner droplet for Ca_2 = 0.05, 0.15 and 0.25. In contrast to the results from the outer droplet, D_1 monotonically increases with Ca_2 increasing, and increasing φ leads to a greater deformation. For the case at Ca_2 = 0.05, the steady-state shape of the inner droplet can be obtained. The influence of Ca_2 on the orientation of the inner droplet is more complex, as seen in Fig. 11(b). The inclination angle θ_1 can reach to a steady-state value, i.e., $\theta_1 \approx 0.25\pi$. In this case, the compound droplet is sliding on the solid surface with a steady-state shape. However, the great deformation (Ca_2 = 0.25)

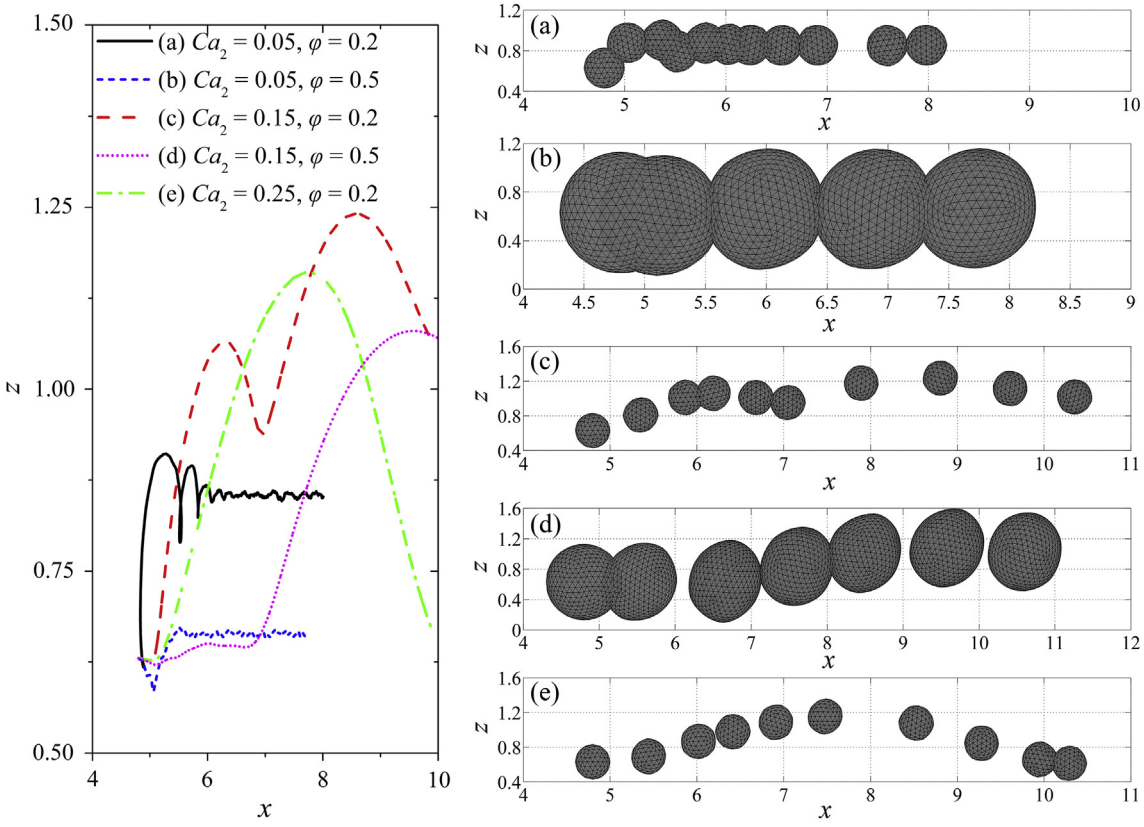

Fig. 12. Trajectories and snapshots of the inner droplet at XZ-plane with considering the effects of Ca_2 and φ.

of the inner interface leads to a large inclination angle, and there are no stable state of deformation and inclination angle exist for a small inner droplet with $\varphi = 0.2$. Because of the rotating motion, it is surprising to find that the orientation angle θ_1 from the inner droplet can be larger than $\pi/4$ even D_1 is only about 0.025 at $Ca_2 = 0.25$. This result could explain the reason why the droplet is more like to be detached or pinched-off at large Ca_2.

Fig. 12 shows the trajectories and shape of the inner droplet with various φ and Ca_2. For sliding case, i.e., Fig. 12(a) and (b), the inner droplet moves toward the downstream in a rotating motion and reach an equilibrium position at the z-axis. The rotating motion vanish when Ca_2 increases to 0.15. Meanwhile, the equilibrium position is found to be closer to the wall as φ increases from 0.2 to 0.5. Consequently, inner droplet stabilize the compound droplet to slide on the solid surface, and prevent it from being detached. With increasing of Ca_2, an induced inclined shear flow drives the inner droplet deforming and moving away from the wall, as seen in Fig. 12(c) and (d). This lateral migration along the z-axis is essential to the onset of detachment. In consideration of the deformation from the outer interface, as seen in Fig. 10, the small inner droplet could promote the elongation of the outer interface (Fig. 10(c)), and then accelerates the onset of pinch-off. Moreover, the greater deformation of the large inner droplet induces a strong induced inclined flow and hinders the lateral migration of the inner droplet. On the other hand, decreasing of Ca_2 to a moderate value, the large inner droplet would promote the detachment. In general, in addition to the deformation of the two interfaces, the lateral migration and the inclination of the inner droplet are dominant factors in determining whether the compound droplet can be pinched-off and detached. The sliding motion is observed at relative large Ca_1, whereas the pinch-off occurs at small Ca_1.

5. Conclusion

We have simulated the deformation and motion of compound droplets adhering to the wall of a rectangular channel under a simple shear flow using the front-tacking method. The effects of the surface tension and inner droplet volume on the compound droplet behavior have been investigated. Our simulations have identified three regimes including sliding, pinch-off and detachment, which have also been observed previously for the homogeneous droplet. Our result also indicates that the dynamics behaviors gain in complexity with increasing capillary number and the volume of inner droplet. It was found that the coupled effect between the interfaces and contact line motion make the dynamics behaviors of compound droplet more complicated than the homogeneous droplet. For small capillary number of the outer interface and inner interface, the sliding motion of compound droplet is subsequently companied by a quasi-steady state. Because of the elongation of the outer interface and lateral migration of the inner droplet, the small droplet accelerates the pinch-off of compound droplet. In contrast, the detachment is preferred to occur for the compound droplet with a large inner droplet. Our results indicate that our theoretical model is of value for understanding the parameters that can affect the compound droplet manipulation and displacement efficiency.

Acknowledgment

Bofeng Bai acknowledges financial support from the Ministry of Science and Technology of the People's Republic of China (Grant no. 2017YFE0100600) and the National Science Fund for Distinguished Young Scholars of China (Grant no. 51425603).

References

Bazhlekov, I.B., Shopov, P.J., Zapryanov, Z.D., 1995. Unsteady motion of a type-A compound multiphase drop at moderate Reynolds numbers. J. Colloid Interf. Sci. 169, 1–12.

Chen, H., Li, J., Shum, H.C., Stone, H.A., Weitz, D.A., 2011. Breakup of double emulsions in constrictions. Soft Matter 7, 2345–2347.

Cox, R.G., 1986. The dynamics of the spreading of liquids on a solid surface. Part 1. Viscous flow. J. Fluid Mech. 168, 169–194.

Dimitrakopoulos, P., 2007. Deformation of a droplet adhering to a solid surface in shear flow: onset of interfacial sliding. J. Fluid Mech. 580, 451–466.

Dimitrakopoulos, P., Higdon, J.J.L., 1998. On the displacement of three-dimensional fluid droplets from solid surfaces in low-Reynolds-number shear flows. J. Fluid Mech. 377, 189–222.

Ding, H., Gilani, M.N., Spelt, P.D., 2010. Sliding, pinch-off and detachment of a droplet on a wall in shear flow. J. Fluid Mech. 644, 217–244.

Ding, H., Spelt, P.D.M., 2007. Inertial effects in droplet spreading: a comparison between diffuse-interface and level-set simulations. J. Fluid Mech. 576, 287–296.

Dupont, J.B., Legendre, D., 2010. Numerical simulation of static and sliding drop with contact angle hysteresis. J. Comput. Phys. 229, 2453–2478.

Ehrhard, P., Davis, S.H., 1991. Non-isothermal spreading of liquid drops on horizontal plates. J. Fluid Mech. 229, 365–388.

Engel, R.H., Riggi, S.J., Fahrenbach, M.J., 1968. Insulin: intestinal absorption as water-in-oil-in-water emulsions. Nature 219, 856–857.

Esmaeeli, A., Tryggvason, G., 1998. Direct numerical simulations of bubbly flows. Part 1. Low Reynolds number arrays. J. Fluid Mech. 377, 313–345.

Fang, C., Hidrovo, C., Wang, F., Eaton, J., Goodson, K., 2008. 3-D numerical simulation of contact angle hysteresis for microscale two phase flow. Int. J. Multiphase Flow 34, 690–705.

Fermigier, M., Jenffer, P., 1991. An experimental investigation of the dynamic contact angle in liquid-liquid systems. J. Colloid Interf. Sci. 146, 226–241.

Gao, P., Feng, J.J., 2011. Spreading and breakup of a compound drop on a partially wetting substrate. J. Fluid Mech. 682, 415–433.

Hochmuth, R., Ting-Beall, H., Beaty, B., Needham, D., Tran-Son-Tay, R., 1993. Viscosity of passive human neutrophils undergoing small deformations. Biophys. J. 64, 1596–1601.

Hua, H., Shin, J., Kim, J., 2014. Dynamics of a compound droplet in shear flow. Int. J. Heat Fluid Flow 50, 63–71.

Huang, H., Liang, D., Wetton, B., 2004. Computation of a moving drop-bubble on a solid surface using a front-tracking method. Commun. Math. Sci. 2, 535–552.

Langer, R., 1998. Drug delivery and targeting. Nature 392, 5–10.

Li, Y., Yun, A., Lee, D., Shin, J., Jeong, D., Kim, J., 2013. Three-dimensional volume-conserving immersed boundary model for two-phase fluid flows. Comput. Method Appl. M 257, 36–46.

Luo, Z.Y., Bai, B.F., 2016. Dynamics of nonspherical compound capsules in simple shear flow. Phys. Fluids 28, 101901.

Luo, Z.Y., He, L., Bai, B.F., 2015. Deformation of spherical compound capsules in simple shear flow. J. Fluid Mech. 775, 77–104.

Luo, Z.Y., Shang, X.L., Bai, B.F., 2018. Marangoni effect on the motion of a droplet covered with insoluble surfactant in a square microchannel. Phys. Fluids 30, 077101.

Muradoglu, M., Tasoglu, S., 2010. A front-tracking method for computational modeling of impact and spreading of viscous droplets on solid walls. Comput. Fluids 39, 615–625.

Ni, M.-J., Komori, S., Morley, N., 2003. Projection methods for the calculation of incompressible unsteady flows. Numer. Heat. Tr B-Fund. 44, 533–551.

Palaniappan, D., Daripa, P., 2000. Compound droplet in extensional and paraboloidal flows. Phys. Fluids 12, 2377–2385.

Park, J.K., Kang, K.H., 2012. Numerical analysis of moving contact line with contact angle hysteresis using feedback deceleration technique. Phys. Fluids 24, 042105.

Peskin, C.S., 2003. The immersed boundary method. Acta Numer. 11, 479–517.

Qian, T., Wang, X.-P., Sheng, P., 2003a. Generalized navier boundary condition for the moving contact line. Commun. Math. Sci. 1, 333–341.

Qian, T., Wang, X.-P., Sheng, P., 2003b. Molecular scale contact line hydrodynamics of immiscible flows. Phys. Rev. E 68, 016306.

Shang, X.L., Luo, Z.Y., Gatapova, E.Y., Kabov, O.A., Bai, B.F., 2018. GNBC-based front-tracking method for the three-dimensional simulation of droplet motion on a solid surface. Comput. Fluids 172, 181–195.

Shintaku, H., Kuwabara, T., Kawano, S., Suzuki, T., Kanno, I., Kotera, H., 2007. Micro cell encapsulation and its hydrogel-beads production using microfluidic device. Microsyst. Technol. 13, 951–958.

Smith, K., Ottino, J., de la Cruz, M.O., 2004. Encapsulated drop breakup in shear flow. Phys. Rev. Lett. 93, 204501.

Smith, K., Solis, F., Tao, L., Thornton, K., De La Cruz, M.O., 2000. Domain growth in ternary fluids: a level set approach. Phys. Rev. Lett. 84, 91.

Spelt, P.D.M., 2005. A level-set approach for simulations of flows with multiple moving contact lines with hysteresis. J. Comput. Phys. 207, 389–404.

Spelt, P.D.M., 2006. Shear flow past two-dimensional droplets pinned or moving on an adhering channel wall at moderate Reynolds numbers: a numerical study. J. Fluid Mech. 561, 439–463.

Stone, H., Leal, L., 1990. Breakup of concentric double emulsion droplets in linear flows. J. Fluid Mech. 211, 123–156.

Sugiyama, K., Sbragaglia, M., 2007. Linear shear flow past a hemispherical droplet adhering to a solid surface. J. Eng. Math. 62, 35–50.

Tasoglu, S., Kaynak, G., Szeri, A.J., Demirci, U., Muradoglu, M., 2010. Impact of a compound droplet on a flat surface: a model for single cell epitaxy. Phys. Fluids 22, 082103.

Tryggvason, G., Bunner, B., Esmaeeli, A., Juric, D., Al-Rawahi, N., Tauber, W., Han, J., Nas, S., Jan, Y.J., 2001. A front-tracking method for the computations of multiphase flow. J. Comput. Phys. 169, 708–759.

Utada, A., Lorenceau, E., Link, D., Kaplan, P., Stone, H., Weitz, D., 2005. Monodisperse double emulsions generated from a microcapillary device. Science 308, 537–541.

Vasudevan, T.V., Naser, M.S., 2002. Some aspects of stability of multiple emulsions in personal cleansing systems. J. Colloid Interf. Sci. 256, 208–215.

Wang, L., Huang, H.-B., Lu, X.-Y., 2013. Scheme for contact angle and its hysteresis in a multiphase lattice Boltzmann method. Phys. Rev. E 87, 013301.

Yamamoto, Y., Ito, T., Wakimoto, T., Katoh, K., 2013. Numerical simulations of spontaneous capillary rises with very low capillary numbers using a front-tracking method combined with generalized Navier boundary condition. Int. J. Multiphase Flow 51, 22–32.

Yamamoto, Y., Tokieda, K., Wakimoto, T., Ito, T., Katoh, K., 2014. Modeling of the dynamic wetting behavior in a capillary tube considering the macroscopic–microscopic contact angle relation and generalized Navier boundary condition. Int. J. Multiphase Flow 59, 106–112.